The Principal Components of Natural Images Revisited

Gunther Heidemann

Abstract—This paper investigates the principal components (PCs) of natural gray and color images. A horizontal and vertical typology of PCs is found which leads to the identification of groups of basis functions for steerable bandpass filters. Using this system, the contribution of spatio-chromatic structure to the total variance can be quantified for selected spatial frequencies.

Index Terms—Statistical image representation, feature measurement, feature representation, texture, color scene analysis, shape, computer vision, computational models of vision, connectionism and neural nets.

1 Introduction

THE principal components (PCs) of natural images are the basic statistical description of the visual appearance of our surroundings: In neurobiology, unsupervised single cell learning rules of Hebbian type mostly lead to an extraction of the PCs [16], [21]; mechanisms of this kind are supposed to be a fundamental principle for the formation of receptive fields in the mammalian early visual system [1]. In computer vision, projection onto PCs is a standard method for feature extraction (e.g., [24]). Hancock et al. have computed the PCs of square patches of natural images [8]. The PCs of such patches which were sampled at random positions from a large, mixed collection of natural images will be addressed as "natural PCs." In [8], the first 15 PCs of a rather small set of images are computed, which does not allow generalization. Using increased computational power, here, a far greater number of PCs is computed in better resolution and from larger databases, revealing a scheme in which natural PCs are organized: PCs form groups of steerable basis functions encoding Gabor-like filters. The same scheme can be found for color images if channels are demixed. Thus, the contribution of spatio-chromatic structure to the total variance can be quantified for selected spatial frequencies.

2 Natural Gray Value PCs

2.1 PC-Computation

As a database, from the high resolution section of [15], five sets of 100 images each were selected at random. For each of the image sets, PCs were computed in the same way as in [8]: Patches of 128×128 pixels were sampled at random positions, every patch of $N_p = 128^2$ pixels is considered as a d-dimensional vector $\vec{x}' \in \mathbb{R}^d$, where $d = N_p$ for gray values and $d = 3N_p$ for color. Every patch was masked, i.e., multiplied pixelwise, with a Gaussian of width $\sigma = 20$ pixels, so the visual stimulus becomes localized and the influence of borders is attenuated. The mean gray level of the sample images was subtracted, then $\vec{x}'$ was normalized to unit length to obtain the final training vector $\vec{x}$. Due to the high dimensionality, only the PCs of large eigenvalues were computed by the neural algorithm of [21], with the only difference that neurons were not trained simultaneously but successively. Neurons were trained one by one over 10^6 samples each, with stepsize ε decreasing exponentially from 10^{-1} to 10^{-5} (see [21]).

• *The author is with the Department of Electrical and Computer Engineering, Florida A&M University, Florida State University, 2525 Pottsdamer St., Tallahassee, FL 32310. E-mail: gh@eng.fsu.edu.*

Manuscript received 24 Aug. 2004; revised 8 Aug. 2005; accepted 22 Aug. 2005; published online 13 Mar. 2006.
Recommended for acceptance by P. Torr.
For information on obtaining reprints of this article, please send e-mail to: tpami@computer.org, and reference IEEECS Log Number TPAMI-0450-0804.

For one of the image sets, the 200 PCs of the largest eigenvalues were computed, for the rest of the image sets, 50 PCs were computed. It was now checked that the obtained PCs are "natural" in the sense that they do not depend on the particular image selection as long as it is well mixed. For this purpose, visual inspection is not sufficient because the eigenvalue spectrum (which is practically identical for all image sets) exhibits several plateaus, as visible in Fig. 1A. In the "degenerate case" of almost identical eigenvalues, neighboring PCs tend to mix linearly or to swap places; an example of two such PCs is shown in Fig. 1B. But, the subspace spanned by the (orthogonal) PCs on an eigenvalue plateau is always the same, independent of the particular image set. This has been checked numerically to ensure that all five sets of PCs actually span the same space.

2.2 Typology of PCs

Fig. 2 shows the gray PCs of the largest eigenvalues (cf. [8] for the first 15). For decreasing eigenvalues, spatial frequency increases since the spectral power of natural images falls with spatial frequency f according to a power law $1/f^p$ [23]. Obviously, the PCs exhibit a certain organization: e.g., PCs 2 and 3 of Fig. 2 are rotated versions of the same function. The same applies, e.g., to PC-pairs (13, 14), (20, 21), or (31, 34). Apart from this "horizontal" organization among PCs of *similar* eigenvalues, a "vertical" one for PCs of very *different* eigenvalues also exists: e.g., PCs 5, 10, 16, 24, 31, 41 resemble a "propeller" with $2, 3, \ldots 7$ blades, respectively. To introduce an intuitive identifier, these PCs will be called "P-type." An additional integer denotes the number of "blades"; rotated versions will be denoted by superscripts "$+$ and "$-$." So, e.g., PCs 10 and 11 are denoted $P3^+$ and $P3^-$, respectively.

Fig. 2 introduces the nomenclature for the PC-types: I "impulse," B "bars," P "propeller," DP "double propeller" (meaning an inner and a phase-shifted outer one), and TP "triple propeller." PCs 2 and 3 can be classified both as B or P. In Fig. 2, identifiers in parentheses (e.g., $(B4)$) denote PCs which cannot be recognized for their type due to linear mixing on an eigenvalue plateau. Fig. 1B shows an example for linear (de)mixing of $B4$. For small eigenvalues, typology becomes more complicated and mixtures of neighboring PCs more likely since the spectrum is flat, e.g., PCs 29 and 30 are mixtures of $B5^+$ and $B5^-$, respectively.

2.3 PCs as a Steerable Basis of Bandpass Filters

The regular shapes of natural PCs call for comparison with meaningful functions, e.g., P-type PCs resemble basis functions for rotationally steerable filter kernels proposed in [5], [18], which suggests searching for such basis functions systematically. A function F is called *rotationally steerable* if versions $F(\alpha)$, which are rotated in the image plane by an arbitrary angle α, can be generated as a linear superposition from a set of basis functions. F is "steered," i.e., rotated, only by changing the weighting coefficients of the basis functions. Preferably, the set of basis filters is small: The major benefit of steerability is that, from the responses of the basis filters to a particular input pattern, the response of $F(\alpha)$ for *any* angle α can also be computed [5].

Easily, for P, DP and TP-type PCs, the "$+$" and "$-$" version can be found to be a steerable basis for arbitrarily rotated versions of themselves. Because of the similarities to the basis functions of [18], groups of neighboring PCs were tested as to whether they are steerable bases of bandpass filters. This was done as follows:

1. Choose plausible parameters of a "target" Gabor wavelet (e.g., such that it resembles a B-type PC of similar eigenvalue).
2. Reconstruct the target by the candidate basis.
3. If this is possible sufficiently well, make rotated versions of the target reconstruction and try to reconstruct it again by superposition of the PCs in the candidate basis.
4. Try to improve reconstruction by modifying Gabor parameters.

By this means, among the first 34 PCs, six groups or "families" can be identified, each of which is the basis of a rotationally steerable, orientation sensitive bandpass filter of Gabor-like shape.

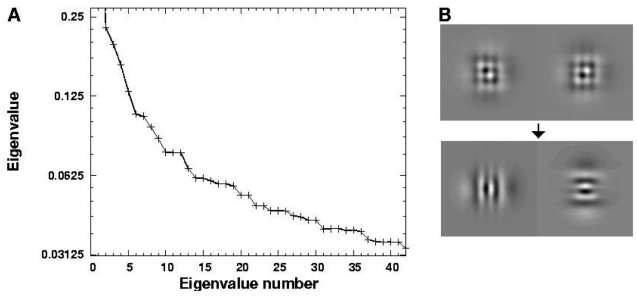

Fig. 1. A: Eigenvalue spectrum of the gray value PCs of Fig. 2 on logarithmic scale. The largest eigenvalue (not shown) is normalized to 1. On plateaus, PCs tend to mix linearly. B: Mixing: PCs 22 and 23 have identical eigenvalues, linear demixing shows they have type $B4$.

These filters will be denoted by S_1, S_1^*, S_2, S_2^*, S_3, and S_3^*. The numbers denote increasing spatial frequency, superscript "$*$" denotes an even filter, while odd filters have no superscript. Even filters exhibit an extremum at the center, odd filters a zero crossing. Fig. 3 depicts the families and the spanned rotationally steerable filters, Table 1 lists the involved types of PCs to point out the systematics. To describe the shape of the generated steerable filters, Table 1, right part, lists the parameters of Gabor functions which fit best the steerable filters S. The notation follows [19]: λ is the wavelength, σ the standard deviation of the Gaussian, γ the spatial aspect ratio, φ the phase, θ the orientation, and b the half-response spatial frequency bandwidth, measured in octaves.

The search for families beyond S_3^* is difficult because the eigenvalue spectrum becomes very flat. Mixtures of neighboring PCs are the rule, so types cannot be identified for a directed search for families. According to the systematics of Table 1, the basis of the next steerable filter, S_4, should include types $B4^+$, $B4^-$, $TP3^+$, $TP3^-$, $DP5^+$, $DP5^-$, $P7^+$, $P7^-$. Except for $TP3^{+,-}$, all of these functions can be found: PCs 22, 23 can be demixed to $B4^{+,-}$, PCs 37, 38 are $DP5^{+,-}$, and PCs 41, 42 are $P7^{+,-}$. For PCs beyond number 50, hardly any specific types can be found (Fig. 4, left). PCs of very small eigenvalues take on a grid-like structure with a high resolution in the center and lower resolution of the surroundings.

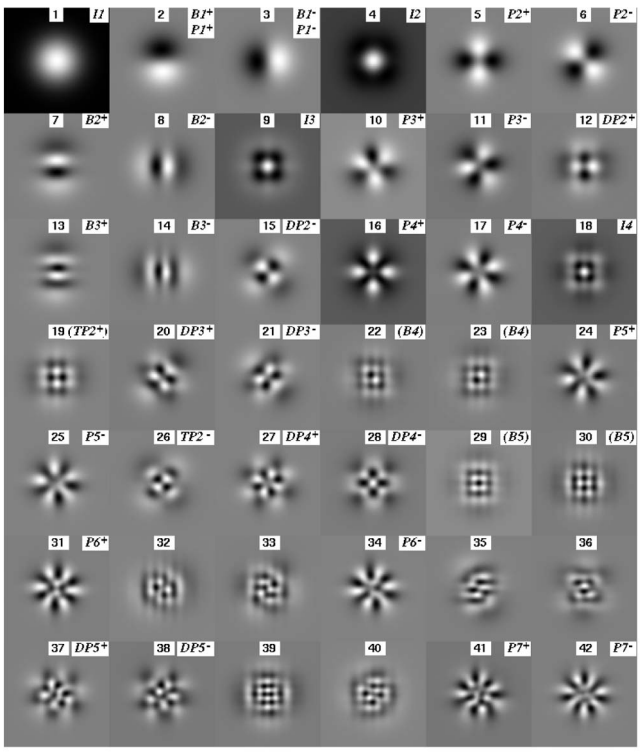

Fig. 2. The first 42 natural PCs, ordered by eigenvalues, with identifiers (Section 2.2).

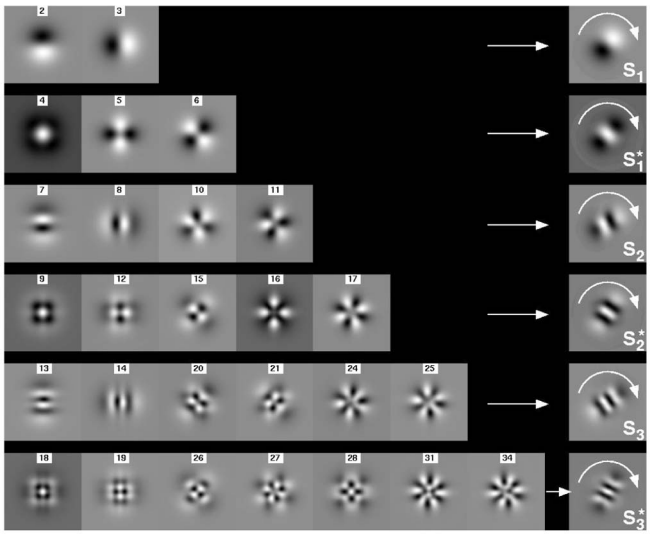

Fig. 3. Families $S_1 \ldots S_3^*$: Each family (row) spans a rotationally steerable filter of a particular frequency and phase, an example of which is shown at an arbitrary angle (right).

Since families $S_1, S_1^* \ldots S_3^*$ complement each other in frequency and phase, it was investigated what kind of filters can be generated when they are combined to form a larger basis. It turns out that, in addition to the filters spanned by the isolated families, orientation sensitive bandpass filters can be generated which are steerable not only in rotation, but also in spatial frequency, phase, and aspect ratio. The range of accessible spatial frequencies is limited to the minimum and maximum values given by S_1 and S_3^*, respectively. Phase can be varied continuously from 0 to 2π, the aspect ratio from about 0.52 to 1.75 (examples in Fig. 4, right).

3 Analysis of Color PCs

Generalization to color was carried out on the same image sets, which were now converted to the perceptually uniform $L^*a^*b^*$ color space (see standard textbooks for the conversion). Since the aim of this paper is primarily to prove the value of spatio-chromaticity for Computer Vision, a color space has to be used which can be easily obtained from the camera output. To keep as close as possible to biological findings, among these color spaces $L^*a^*b^*$ is chosen as the one which is closest in thought to biological findings: First, Euclidian distance in the $L^*a^*b^*$ approximately corresponds to perceived color distance. Second, the use of one achromatic axis and two opponent color axes (yellow-blue, red-green) corresponds to results from [3], [20]. In [20], the responses of photoreceptors are computed from hyperspectral images using a model of spectral cone sensitivity (Stockman-MacLeod-Johnson). In the resulting space of cone response values, one achromatic and two chromatic principal axes (again yellow-blue, red-green) turn out to be sufficient to capture most of the color variance.

The aim of the present work is an analysis of the spatio-chromatic *structure*, whereas earlier investigations of natural color PCs were aimed at the accurate reproduction of natural color principal axes [3], [20], [25]. These works consistently showed the split up into three axes, but used too little spatial resolution for detailed spatio-chromatic analysis. Here, using the $L^*a^*b^*$ space, a different way is chosen: The fact that one achromatic and two opponent color axes are an adequate color representation is taken for granted; the effort is spent on the spatial structure instead.

The results for color PCs are confusing at first glance (Fig. 5, left): Though some of the gray value PC-types can be found, the majority of natural color PCs are a mess of colored spots difficult to interpret. Moreover, when color PCs are computed on different image sets, the resulting PCs appear quite different every time. This effect is caused

TABLE 1
Scheme of PC-Families ($I1$ Included as "S_0^*" for Clarity)

Fa.	PCs								λ	σ	γ	φ	b
S_0^*	$I1$								∞	19.6	1	0	–
S_1	$B1^+$	$B1^-$							68.3	23.7	1.75	1.56	1.74
S_1^*	$I2$						$P2^+$	$P2^-$	49.9	21.0	1.69	–0.01	1.38
S_2	$B2^+$	$B2^-$					$P3^+$	$P3^-$	34.2	19.9	1.71	1.71	0.97
S_2^*	$I3$				$DP2^+$	$DP2^-$	$P4^+$	$P4^-$	26.6	18.5	1.67	0.12	0.80
S_3	$B3^+$	$B3^-$			$DP3^+$	$DP3^-$	$P5^+$	$P5^-$	19.4	15.0	1.41	1.56	0.73
S_3^*	$I4$		$TP2^+$	$TP2^-$	$DP4^+$	$DP4^-$	$P6^+$	$P6^-$	16.8	14.0	1.48	–0.02	0.66
(S_4)	$B4^+$	$B4^-$	$(TP3^+)$	$(TP3^-)$	$DP5^+$	$DP5^-$	$P7^+$	$P7^-$	–	–	–	–	–

Basis sets of even filters start with an I-type PC, basis sets of odd filters with B^+, B^--type PCs. For $S4$, the hypothesized $TP3^{+,-}$ functions could not be found in isolation because the eigenvalue spectrum is too flat. Right: Parameters of the best fit Gabor functions. Note, for pairs S_i, S_i^*, phases differ by $\Delta\varphi \approx \pi/2$.

by the eigenvalue spectrum, which exhibits three times broader plateaus than in the gray value case. Since the computations lead to arbitrary linear superpositions of PCs on eigenvalue plateaus, the difficulty in recognizing the known PC-types becomes understandable. Consequently, it makes sense to search for the PC-shapes known from the gray value case by a linear "demixing" of PCs on eigenvalue plateaus. For example, PCs number 6-9 of Fig. 5, left, resemble the known typology; by linear demixing, the PCs can be decomposed such that PC 6 becomes $I2$ of luminance, PC 7 becomes $P1^+$ of yellow-blue, etc., see Fig. 5, right.

The demixing procedure is based on minimization of a cost function E. The application of E can be seen best by an example: PCs 11 and 12 appear to be a mixture of $B2^+$ of luminance and $B1^+$ of red-green. To obtain a demixed basis $\vec{W}', \vec{W}'_\perp$ spanning the same subspace as PCs 11 and 12, superpositions $\vec{W}'$ of PCs 11 and 12 are formed such that E is minimized, where E is the pixelwise mean square difference between $\vec{W}'$ and a gray value version of $B2^+$. Once the optimal $\vec{W}'$ has been found, the orthogonal vector $\vec{W}'_\perp$ within the subspace spanned by PCs 11 and 12 can be computed, which is now a red-green version of $B1^+$. In case PC-shapes cannot be guessed, an alternative definition of E is the average color saturation of $\vec{W}'$—minimization of E then leads to "decoloring" of $\vec{W}'$ while "concentrating" color in $\vec{W}'_\perp$. Such separation of luminance and color leads to the same result. To demix plateaus of more than two PCs, stepwise demixing of only two PCs at a time is easiest, using different optimization criteria in turn to demix the complete plateau.

In the demixed PCs (Fig. 5, right), the expected three independent "channels" of PCs can be identified: luminance, yellow-blue, and red-green. Note the color pairings do not exactly reflect the $L^*a^*b^*$-axes, but are a result of the natural color statistics. For each channel, the same typology applies as for gray imagery. As a consequence, the steerable filters $S_1 \ldots S_3^*$ known from gray values can be spanned in color. Eigenvalues differ for the three channels. Luminance has the largest eigenvalues, red-green the smallest, i.e., each type of PC occurs later in the spectrum for red-green than for luminance, e.g., $P2^+$ is at position 8 for luminance, but at position 18 for yellow-blue and at 31 for red-green. So, though the PCs of each channel code the same pattern types, their quantitative contributions to natural patterns are different. The demixed color PCs allow computation of these contributions for selected spatial frequencies.

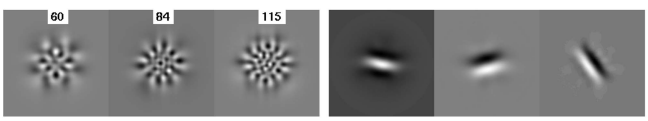

Fig. 4. Left: PCs of small eigenvalues. Particular structures can hardly be made out because the eigenvalue spectrum is flat. Right: The combined basis of families $S_1 \ldots S_3^*$ spans filters steerable also in phase, frequency, and aspect ratio. Examples are shown for parameters similar to those of simple cells: aspect ratio $\gamma = 0.52 - 0.68$, bandwidth $b = 1.65 - 2.45$.

4 Discussion

Natural PCs have been found to form a steerable basis of bandpass filters—however, provided a sufficiently large basis, *every* function can be generated and steered in rotation as long as it is band-limited in angular frequency [5]. What makes natural PCs "special" as a basis is the combination of four facts:

1. A very *small* number of basis functions is sufficient to span a rotationally steerable filter, i.e., each basis is highly specialized to generate just this filter type.
2. *All* of at least the first 31 PCs belong to such a group of basis functions.
3. *All* of the spanned filters are bandpass.
4. The filters *complement* each other in frequency and phase to form a larger basis for edge, bar, and grating-like patterns with several steerable parameters.

The results were found for well-mixed imagery, whereas, for specialized image domains such as "buildings" or "fireworks," the PCs differ in order and by mixing. Though, in principle, such "nonnatural" PCs can still span Gabor functions, the Gabors are more "spread out" over the basis, i.e., many more PCs are needed as a basis, including many of low eigenvalues.

In a natural environment, edge, bar, and grating-like patterns contribute most to variance. So far, edge or bar-filters were mostly computed from natural imagery using methods which exploit higher order statistics such as independent component analysis (ICA) [17], [2]. The fact that such patterns are also captured by second order statistics can be easily overlooked because these patterns are represented in the first natural PCs in a highly effective, compressed way. As the PCs do not capture prototypes, but orthogonal directions of maximum variance, most of the encoded patterns do not become visible in the basis itself. Thus, only *single* PCs were found to be similar to cortical receptive fields in [8], but not yet *all* PCs were realized to contribute to the complete set of orientations. A major difference, however, between PCs and filters obtained by algorithms exploiting higher order statistics (which use PCA for "whitening" in preprocessing to remove second order statistics) is that higher order statistics yields *localized* filters, whereas here locality is introduced by windowing.

Part of the results found here experimentally can be understood from statistical considerations. If the statistics are translation invariant—i.e., pixel correlations depend only on the distance, not (absolute) location—the PCs become Fourier components (e.g., [17]) because the sampling process is stationary. The eigenvalues will reflect the mentioned power law $1/f^p$ [23]. But, the Gaussian windowing breaks the translational symmetry and imposes rotational symmetry, provided the image statistic itself is rotationally invariant. If so, the PCs can be separated into a product of radial, rotationally invariant functions, and angular functions. The radial functions are the Fourier components for cylindrical systems, the Hankel functions [13]. However, though the I-type PCs suggest that the radial component is governed by Hankel functions, an exact fit could not be found; the reasons are probably linear mixing and the nonperfect rotational invariance of natural imagery.

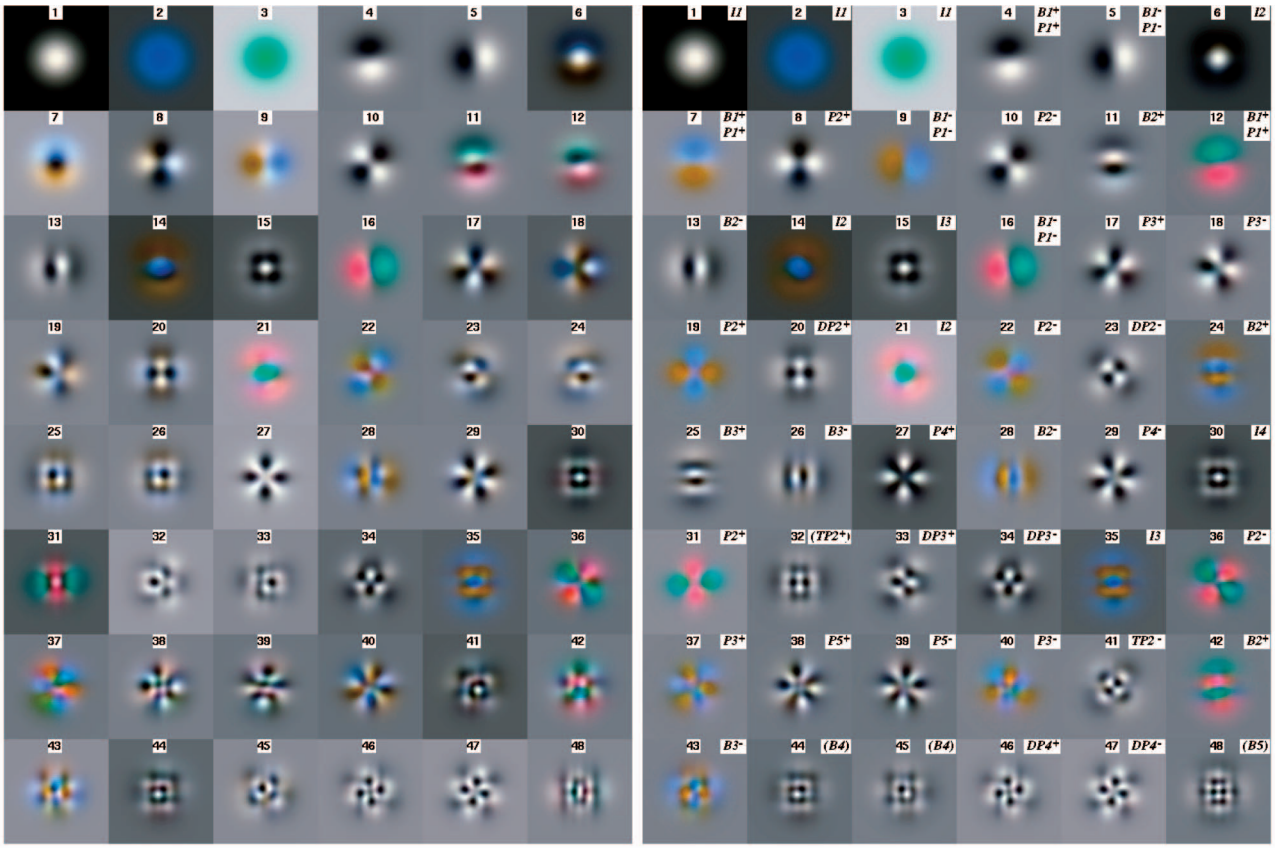

Fig. 5. Left: The first 48 natural color PCs, as obtained "raw" from the computation. Due to broad eigenvalue plateaus, PCs are mixed, only some types can be identified. Right: After linear demixing (separately on each eigenvalue plateau), all types of the gray value PCs are present for luminance and the two opponent color channels.

4.1 Spatio-Chromatic Features for Computer Vision

According to the "coloring book theory," visual form is believed to be perceived only from luminance, whereas the role of color is limited to filling perceived forms subsequently [14]. The coloring book theory has been established from early findings of biological vision, but its influence is also still great on computer vision. Even in the domain of content-based image retrieval (CBIR), where color is used more extensively than in other branches of computer vision, form is mostly evaluated from gray values only, whereas color is, e.g., summed up in histograms, discarding spatial information.

From the point of view of second order statistics, a vision system that perceives form only from luminance and exploits color just to fill in form later would only be justified if color PCs were arranged in the following way: Most of the chromatic variance would be assembled in the first, spatially unstructured chromatic PCs (numbers 2 and 3 in Fig. 5), whereas the other, spatially structured chromatic PCs would have much smaller eigenvalues and therefore appear much later—gray PCs would dominate by far. But, results literally paint a different picture: Though gray PCs dominate, among the first 40 spatially structured PCs of Fig. 5, right, there are 17 chromatic (PCs 1-3 are not considered). Contributions of the spatio-chromatic PCs to the total variance sum up to about 41 percent (gathered from the eigenvalue spectrum). Therefore, spatial physical structure expresses itself in imagery comparably strong in spatio-chromatic features as in luminance. Moreover, spatio-chromatic channels are dominated by the same edge, bar, and grating-patterns as luminance.

Consequently, spatio-chromatic features are not much less well-suited for form perception than luminance. Moreover, recent results in biological vision indicate that V1 neurons indeed exploit spatial color features for form perception [11], [6], so the originally biological motivation becomes questionable. The strong presence of spatio-chromatic structure gives rise to reconsidering the role of color features for form evaluation. Encouraging results on the use of spatio-chromatic features were already achieved, e.g., using steerable Gaussian derivatives [7] or spatio-chromatic filter masks obtained by local PCA in the context of CBIR [9].

Spatio-chromatic features are particularly valuable for applications because of the robustness to translation. This property becomes obvious from the order of spatial frequencies: For the same eigenvalue, the corresponding color PC has lower spatial frequency than the gray value PC (compare, e.g., PCs 31 and 32 of Fig. 5, right). Features of low spatial frequency are preferable for many vision tasks because they are more robust against translation or image distortion. In other words, if, for a given technical or biological vision task, a certain representational power is required, the first n PCs of all three channels make the more stable features than the first n gray value PCs. Note also the relation to *compression*: Nonadaptive compressors rely on predefined basis function families which are usually ordered into groups spanning different spatial frequencies, e.g., the discrete cosine transform (DCT) is applied for JPEG (motivated by the relation to PCA). If an incomplete set of basis functions is to be selected for lossy compression, measures for the relevance of different basis functions are required. Estimation of the chromatic variance contribution allows a quantitative relevance comparison of the three channels for selected spatial frequencies.

4.2 Potential Implications for Biological Vision

Though technical not biological vision is the main focus of this paper, possible relations to biology will be pointed out. The discussion is restricted to the gray value case because the $L^*a^*b^*$ color space is an insufficient approximation of the cone responses. Visual receptive fields (RFs) that resemble natural PCs were not found in neurophysiology. Rather, simple cells in the primary visual cortex, e.g., of cats [10], are sensitive to edges, bars, and gratings. Their RFs can be modeled by orientation sensitive bandpass filters [12]. Simple cells appear to form a sparse, overcomplete representation of the input. It has been shown that sparseness constraints can explain simple cell like RFs [17] and that

sparseness can be formalized by Independent Component Analysis (ICA) [2]. For the case of color, ICA leads to the same split up into opponent color channels for RGB [22] and hyperspectral images [25] observed here.

The current work cannot judge if "PC-neurons" might exist in spite of the neurophysiological evidence, but it should be pointed out that hypothetical PC-neurons would make an exceptionally good basis for *wiring* a layer of simple cells: PC-neurons would be able to represent visual patterns coming from the retina in a compressed form before information spreads out to the known, overcomplete representation by simple cells in the cortex. Thus, only minimal wiring would be required from a layer of PC-neurons to a layer of simple cells. A group of a few PC-neurons could serve as a steerable basis for a much larger group of simple cells which represent the respective Gabor-like RF in an arbitrary number of orientations by giving simply different weightings to the PC-neurons. Note the basis of PC-neurons might look different among individuals due to mixing on eigenvalue plateaus.

The hypothesis is plausible insofar as the half-response spatial frequency bandwidth $b = 0.66 - 1.74$ octaves for PC-based filters is within the observed range of, e.g., $0.4 - 2.6$ for macaque monkey simple cells [4] (cf. Table 1). But, the observed spatial aspect ratio γ, which characterizes the eccentricity of the RF-ellipse, does not match for single families $S_1 \dots S_3^*$: $\gamma \approx 1.41 - 1.75$ (Table 1), whereas values $0.23 - 0.92$ were found for simple cells [12]. So, the main difference is that steerable filters generated from *single* families are more longish (in the direction of the wavevector) than simple cell RFs. But, such filters can be generated very well from the natural PCs if the families are *combined* as described above: For the joint basis of families $S_1 \dots S_3^*$, Gabor filters with aspect ratios γ in the range of $0.52 - 1.75$ and bandwidths b in the range of $0.66 - 2.45$ can be generated, as illustrated in Fig. 4, right. Thus, it is possible to span simple cell RFs observed in neurophysiology using the complete set of PCs up to number 34 as basis functions. Note, however, that there are more patterns than Gabor-like ones within the span of this set of basis functions.

REFERENCES

[1] H.B. Barlow, "Possible Principles Underlying the Transformations of Sensory Messages," *Sensory Comm.*, pp. 217-234, MIT Press, 1961.

[2] A.J. Bell and T.J. Sejnowski, "The Independent Components of Natural Images Are Edge Filters," *Vision Research*, vol. 37, no. 27, pp. 3327-3338, 1997.

[3] G. Buchsbaum and A. Gottschalk, "Trichromacy, Opponent Colour Coding and Optimum Colour Information Transmission in the Retina," *Proc. Royal Soc. London B*, vol. 220, pp. 89-113, 1983.

[4] R.L. de Valois, D.G. Albrecht, and L.G. Thorell, "Spatial Frequency Selectivity of Cells in Macaque Visual Cortex," *Vision Research*, vol. 22, pp. 545-559, 1982.

[5] W.T. Freeman and E.H. Adelson, "The Design and Use of Steerable Filters," *IEEE Trans. Pattern Analysis and Machine Intelligence*, vol. 13, pp. 891-906, 1991.

[6] K. Gegenfurtner, "Color in the Cortex Revisited," *Nature Neuroscience*, vol. 4, no. 4, pp. 339-340, 2001.

[7] D. Hall, J.L. Crowley, and V. Colin de Verdière, "View Invariant Object Recognition Using Coloured Receptive Fields," *Machine Graphics and Vision*, vol. 9, no. 2, pp. 341-352, 2000.

[8] P.J.B. Hancock, R.J. Baddeley, and L.S. Smith, "The Principal Components of Natural Images," *Network*, vol. 3, pp. 61-70, 1992.

[9] G. Heidemann, "Combining Spatial and Colour Information for Content Based Image Retrieval," *Computer Vision and Image Understanding*, vol. 94, nos. 1-3, pp. 234-270, 2004.

[10] D.H. Hubel and T.N. Wiesel, "Receptive Fields, Binocular Interaction, and Functional Architecture in the Cat's Visual Cortex," *J. Physiology*, vol. 160, pp. 106-154, 1962.

[11] E.N. Johnson, M.J. Hawken, and R. Shapley, "The Spatial Transformation of Color in the Primary Visual Cortex of the Macaque Monkey," *Nature Neuroscience*, vol. 4, no. 4, pp. 409-416, 2001.

[12] J.P. Jones and L.A. Palmer, "An Evaluation of the Two-Dimensional Gabor Filter Model of Simple Receptive Fields in Cat Striate Cortex," *J. Neurophysiology*, vol. 58, no. 6, pp. 1233-1258, 1987.

[13] D.J.C. MacKay and K.D. Miller, "Analysis of Linsker's Applications of Hebbian Rules to Linear Networks," *Network*, vol. 1, pp. 257-297, 1990.

[14] D. Marr, *Vision: A Computational Investigation into the Human Representation and Processing of Visual Information*. San Francisco: Freeman, 1982.

[15] Nova Development Corporation, *Art Explosion Photo Gallery*, 2002.

[16] E. Oja, "A Simplified Neuron Model as a Principal Component Analyzer," *J. Math. Biology*, vol. 15, pp. 267-273, 1982.

[17] B.A. Olshausen and D.J. Field, "Emergence of Simple-Cell Receptive Field Properties by Learning a Sparse Code for Natural Images," *Nature*, vol. 381, pp. 607-609, 1996.

[18] P. Perona, "Deformable Kernels for Early Vision," *IEEE Trans. Pattern Analysis and Machine Intelligence*, vol. 17, no. 5, pp. 488-499, May 1995.

[19] N. Petkov and P. Kruizinga, "Computational Models of Visual Neurons Specialised in the Detection of Periodic and Aperiodic Oriented Visual Stimuli: Bar and Grating Cells," *Biological Cybernetics*, vol. 76, no. 2, pp. 83-96, 1997.

[20] D.L. Ruderman, T.W. Cronin, and C.-C. Chiao, "Statistics of Cone Responses to Natural Images: Implications for Visual Coding," *J. Optical Soc. Am. A*, vol. 15, no. 8, pp. 2036-2045, 1998.

[21] T.D. Sanger, "Optimal Unsupervised Learning in a Single-Layer Linear Feedforward Neural Network," *Neural Networks*, vol. 2, pp. 459-473, 1989.

[22] D.R. Tailor, L.H. Finkel, and G. Buchsbaum, "Color-Opponent Receptive Fields Derived from Independent Component Analysis of Natural Images," *Vision Research*, vol. 40, no. 19, pp. 2671-2676, 2000.

[23] D.J. Tolhurst, Y. Tadmor, and T. Chao, "Amplitude Spectra of Natural Images," *Ophthalmic & Physiological Optics*, vol. 12, no. 2, pp. 229-232, 1992.

[24] M. Turk and A. Pentland, "Eigenfaces for Recognition," *J. Cognitive Neuroscience*, vol. 3, pp. 71-86, 1991.

[25] T. Wachtler, T.W. Lee, and T.J. Sejnowski, "Chromatic Structure of Natural Scenes," *J. Optical Soc. Am. A*, vol. 18, no. 1, pp. 65-77, 2001.